Human Platelet Factor 4 Subunit Association/Dissociation Thermodynamics and Kinetics†

Mu-Jung Chen and Kevin H. Mayo*

Department of Chemistry and The Fels Institute for Cancer Research and Molecular Biology, Temple University, Philadelphia, Pennsylvania 19122

Received February 6, 1991; Revised Manuscript Received April 11, 1991

ABSTRACT: Platelet factor 4 (PF4) monomers (7800 daltons) form dimers and tetramers in varying molar ratios under certain solution conditions [Mayo, K. H., & Chen, M. J. (1989) *Biochemistry 28*, 9469]. The presence of a simplified aromatic region (one Tyr and two His) and resolved monomer, dimer, and tetramer Y60 3,5 ring proton resonances makes study of PF4 aggregate association/dissociation thermodynamics and kinetics possible. PF4 protein subunit association/dissociation equilibrium thermodynamic parameters have been derived by ^{1}H NMR (500 MHz) resonance line-fitting analysis of steady-state Y60 3,5 ring proton resonance monomer–dimer–tetramer populations as a function of temperature from 10 to 40 °C. Below 10 °C and above 40 °C, resonance broadening and overlap severely impaired analysis. Enthalpic and entropic contributions to dimer association Gibb's free energy [−5.1 kcal/mol (30 °C)] are +2.5 ± 1 kcal/mol and +26 ± 7 eu, respectively, and for tetramer association Gibb's free energy [−5.7 kcal/mol (30 °C)], they are −7.5 ± 1 kcal/mol and −7 ± 3 eu, respectively. These thermodynamic parameters are consistent with low dielectric medium electrostatic/hydrophobic interactions governing dimer formation and hydrogen bonding governing tetramer formation. Association/dissociation kinetic parameters, i.e., steady-state jump rates, have been derived from exchange-induced line-width increases and from ^{1}H NMR (500 MHz) saturation-transfer and spin–lattice (T_1) relaxation experiments. From dissociation jump rates and equilibrium constants, association rate constants were estimated. For dimer and tetramer equilibria at 30 °C, unimolecular dissociation rate constants are 35 ± 10 s^{-1} for dimer dissociation and 6 ± 2 s^{-1} for tetramer dissociation. The association rate constants at 30 °C are (13 ± 4) × 10^4 and (8 ± 2) × 10^4 M^{-1} s^{-1}, respectively. Activation enthalpies and entropies have been derived from the temperature dependence of forward/reverse rate constants. Kinetically, tetramers are preferred over dimers due primarily to a slower dissociation rate, and thermodynamically, tetramer formation is enthalpy-driven, while dimerization is entropy-driven.

Biological reactions generally involve interactions with protein molecules. While these are too numerous to list, considerable information is available in a number of systems involving static aspects of molecular associations. Much less, however, is known concerning association/dissociation thermodynamics and kinetics, an understanding of which is critical to revealing the molecular mechanistic basis of reactions. These studies are usually limited to small molecule–protein reactions since these are both easier to detect and involve rates accessible by normally employed stopped-flow kinetic techniques. Perhaps to date the most studied protein–protein association reaction involves the α-chymotrypsin dimerization process (Koren & Hammes, 1975; Aune & Timasheff, 1971; Aune et al., 1971; Kitano et al., 1989).

Human platelet factor 4 (PF4),[1] a secretory peptide from α-storage granules, contains 70 amino acid residues (7800 daltons) of which only 3 are aromatic, i.e., His-23, His-35, and Tyr-60 (Deuel et al., 1977, 1981; Hermodson et al., 1977; Walz et al., 1977). PF4 monomers are known to associate in a tetrameric structure at low concentration (50 μg/mL) under physiological conditions (Barber et al., 1972; Moore et al., 1975) and in a distribution of monomer–dimer–tetramer states under certain conditions at higher concentration (milligrams per milliliter) (Mayo & Chen, 1989). Monomer–dimer–tetramer (M–D–T) equilibria have been investigated by ^{1}H NMR spectroscopy (Mayo & Chen, 1989). There, M–D–T resonances demonstrated significant exchange broadening, and NOESY experiments showed magnetization transfer cross-peaks among M–D–T-associated resonances. These observations provide the basis for this present study, by indicating that kinetic exchange parameters for PF4 association/dissociation can be derived from analysis of resonance exchange broadening and ST-NMR experiments.

Saturation-transfer (ST) NMR has been used previously in a number of systems to deduce binding kinetic parameters, but for technical reasons, it has been limited to small molecule–protein interactions (Brown & Owaga, 1977; Cayley et al., 1979). Exemplifying this further, ^{31}P ST-NMR has been used to study small molecule–protein interactions in the creatine kinase/ATP reaction (Ugurbil et al., 1986; Brindle et al. 1984), in the kinetics of *N*-(phosphonacetyl)aspartate interaction with the catalytic subunit of aspartate transcarbamoylase (Cohen & Schachman, 1986), and in the phosphoglucomutase reaction (Post et al., 1989). ^{13}C ST-

†This work was supported by grants from the American Heart Association, Philadelphia Section, and the National Institutes of Health (HL-43194) and benefited from NMR facilities made available to Temple University through Grant RR-04040 from the National Institutes of Health. In partial fulfillment of the Ph.D. requirements of Temple University for M.-J.C.

* Address correspondence to this author at his present address: Department of Pharmacology, Jefferson Cancer Institute, Thomas Jefferson University, Blumerle Life Sciences Building, Philadelphia, PA 19107.

[1] Abbreviations: PF4, platelet factor 4; NMR, nuclear magnetic resonance; NOE, nuclear Overhauser effect; rf, radio frequency; FID, free induction decay; ST, saturation transfer; T_1, spin–lattice relaxation time; M-Y60, tyrosine-60 in the monomer state; D-Y60, tyrosine-60 in the dimer state; T-Y60, tyrosine-60 in the tetramer state; eu, entropy unit (calories per mole per degree kelvin).

0006-2960/91/0430-6402$02.50/0

NMR has been used to study the alanine aminotransferase reaction (Malloy et al., 1985). Similarly, resonance exchange broadening has been most effectively used in studying small molecule–protein interactions, where the concentration dependence of resonance line widths of the ligand in the free and bound states can easily be derived (Jardetzky & Roberts, 1981). In dealing with protein–protein or large molecular interactions, it is normally difficult to establish from the NMR spectrum, for example, which exchange regime one is in and therefore which method of analysis could be used to derive exchange rate information.

While most protein–protein association/dissociations cannot be studied in this fashion, PF4 is exceptional as an ideal model system for using exchange broadening analysis and ST-NMR to study the kinetics and thermodynamics of larger molecular interactions for several reasons: (1) simple downfield aromatic resonance region, i.e., only one Tyr and two His; (2) reasonably resolved Y60 3,5 proton resonances in monomer, dimer, and tetramer states all observable at pH 4; and (3) equilibrium exchange fluxes or jump rates which fall into the appropriate NMR time window for slow intermediate exchange, i.e., aggregate state lifetimes on the order of T_1 values. Only through a combination of these experimental conditions were such studies possible.

Materials and Methods

Isolation of PF4. Outdated human platelets were obtianed from the Red Cross and centrifuged at 10000*g* for 1 h to obtain platelet-poor plasma. This preparation was applied to a heparin–agarose (Sigma) column (bed volume 50 mL); the column was washed with 0.2, 0.5, 1, and 1.5 M NaCl. The fraction eluting at 1.5 M NaCl which yielded most of the PF4 (Rucinski et al., 1979) was then desalted by dialysis (0.2% trifluoroacetic acid). The resulting solution was concentrated by lyophilization. From about 50 units of outdated platelets, 15 mg of PF4 generally resulted.

Protein Concentration. Protein concentration was determined by the method of Lowry et al. (1951), and results were calculated from a standard dilution curve of human serum albumin. An alternative method used to determine PF4 concentration was that of Waddell (1956).

Nuclear Magnetic Resonance (NMR) Spectroscopy. Samples for ^{1}H NMR measurements had been lyophilized and redissolved in ^2H_2O immediately before the experiment. The final protein concentration ranged from 1 to 4 mg/mL as indicated in the text. The p^{2}H was adjusted by adding microliter increments of NaO^2H or ^{2}HCl to a 0.6-mL sample. All measurements were done at the p^{2}H value indicated in the text read directly from the pH meter and not adjusted for isotope effects.

^{1}H NMR spectra were recorded in the Fourier mode on a General Electric GN-omega 500-NMR spectrometer (500 MHz for protons). The solvent deuterium signal was used as a field-frequency lock. All chemical shifts are quoted in parts per million (ppm) downfield from sodium 4,4-dimethyl-4-silapentanesulfonate (DSS).

^{1}H ST-NMR Experiments. Saturation-transfer (ST) ^{1}H NMR experiments were accomplished by irradiating the desired peak for 0.02 s up to 0.4 s, at an rf power level sufficient to null *z* magnetization of the irradiated peak in 0.02 s. A 2-ms delay was introduced before accumulation to reduce transient effects, and a time of 2 s was allowed between the beginning of accumulations to allow for recovery of *z* magnetization. Difference spectra were generated by subtracting the free induction decay (FID) of the irradiated peak spectrum from the FID of a control spectrum which had been irradiated in a region where no resonances occur under the same experimental conditions.

Spin–Lattice Relaxation Experiments. Spin–lattice relaxation (T_1) measurements were performed by selectively irradiating the desired peak at a power level sufficient to null *z* magnetization. The growth of *z* magnetization back to its equilibrium value was followed as a function of time. A 2-s delay was allowed before selective irradiation to allow for complete recovery of *z* magnetization. The data were plotted as first-order kinetics, and the T_1 values were taken from the inverse of the slope.

Gaussian/Lorentzian Line-Shape Analysis. Resonance area integrals were derived by Gaussian/Lorentzian line fitting of NMR spectra. These procedures were done on a Sun Sparc workstation with standard Gaussian/Lorentzian functions. A part of the NMR spectrum containing the frequency region of interest was transferred to the workstation. Initially, chemical shifts and line widths were taken for the monomer resonance acquired at low PF4 concentration and low pH where greater than 90% monomer state exists; for the tetramer resonance, a higher protein concentration was used where the tetramer state predominates. Initial resonance heights were estimated from the position of monomer, dimer, and tetramer resonances which were generally distinguishable. A base line was established by comparing fits with the noise level where no resonances were found on both sides of the aromatic resonance region. Base lines were generally flat. Derived areas from these fits varied from sample to sample by no more than about 10%.

Half-height line widths, $\Delta\nu_{1/2}$, were estimated from Gaussian/Lorentzian lines fitted to M, D, and T-Y60 (3,5) ring proton resonances described above. In cases where resonances did not overlap appreciably, half-height line widths were estimated directly from NMR resonances on the GN-omega-500 spectrometer display. In spectra where Y60 2,6–3,5 proton spin–spin couplings were resolved, i.e., M-Y60 resonances, the normally observed 7–8-Hz $^3J_{\delta\epsilon}$ coupling constants (Wüthrich, 1986) were measured. In estimating $\Delta\nu_{1/2}$ values, these $^3J_{\delta\epsilon}$ values were used and assummed not to change over the temperature range analyzed, i.e., 10–40 °C. Many $\Delta\nu_{1/2}$ values and most $\Delta\nu'_{1/2}$ values, i.e., the apostrophe indicates the presence of exchange, ranged from 30 to 60 Hz and were much greater than $^3J_{\delta\epsilon}$ coupling constants.

Results

Platelet factor 4 (PF4) subunit association/dissociation equilibria can be depicted as shown in eq 1 and discussed by

$$M + M \underset{k_{DM}}{\overset{k_{MD}}{\rightleftharpoons}} D \qquad D + D \underset{k_{TD}}{\overset{k_{DT}}{\rightleftharpoons}} T \qquad (1)$$

Mayo and Chen (1989) where M, D, and T stand for monomer, dimer, and tetramer, respectively. Steady-state exchange rate constants or "jump rates" (inverse lifetime of M, D, or T state) are indicated by *k* with subscripts for the exchange direction, e.g., "MD" for monomer to dimer. It has been shown by Mayo and Chen (1989) that under certain solution conditions, populations of PF4 monomers, dimers, and tetramers in slow exchange on the NMR time scale can be simultaneously observed. Moreover, resonances for Y60, H23, and H35 have been identified and assigned to specific M, D, and T aggregate states (Mayo & Chen, 1989).

It is important to realize here that one is dealing with a three-state exchanging system as shown in eq 1. Normally, the few multisite systems which have been examined by NMR [see Faller (1973) and references cited therein; Mann, 1977; Mamatyuk et al., 1974; Forsen & Hoffman, 1964] were sim-

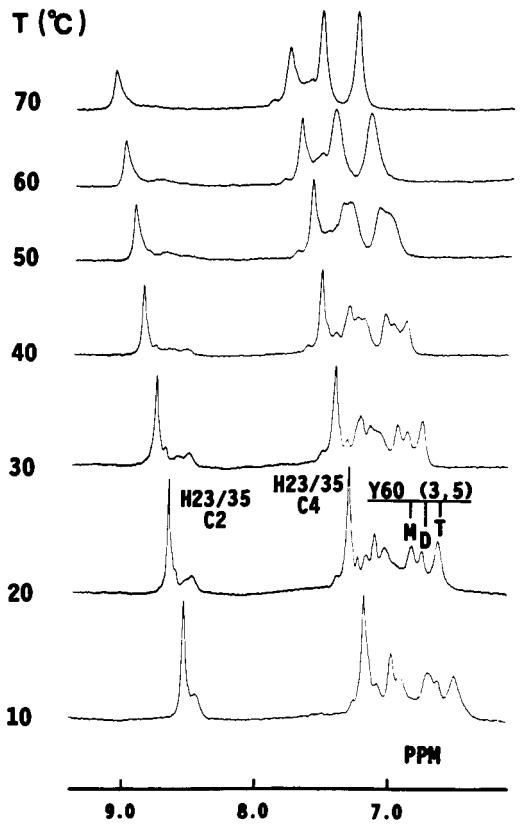

FIGURE 1: PF4 proton NMR spectra temperature dependence. 500-MHz proton NMR spectra of human PF4 are shown as a function of temperature from 10 to 70 °C. Lyophilized PF4 sample was dissolved in ^2H_2O at pH 4, 303 K, containing 3.2 mg/mL PF4. The only salt added came from the minimal amount of NaO^2H and ^2HCl necesary to adjust the solution pH; this NaCl concentration was about 10 μM. No additional buffer or salt was added to these solutions. The resonance label prefixes M, D, and T stand for monomer, dimer, and tetramer, respectively, according to Mayo and Chen (1989). At each temperature, the HDO resonance is set at 4.86 ppm, and spectra are plotted accordingly.

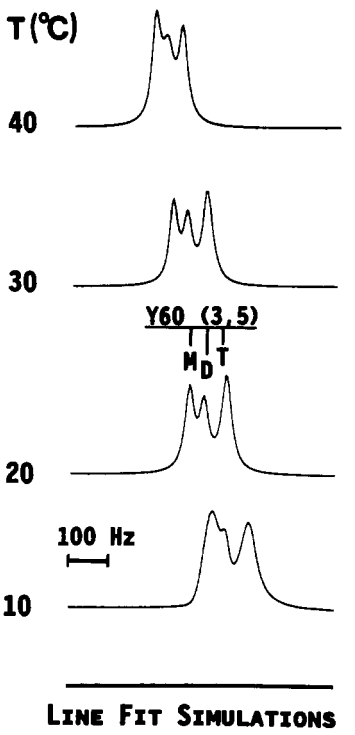

FIGURE 2: Line fitting of M–D–T Y60 3,5 resonances. Summed Gaussian curves for M, D, and T-Y60 3,5 resonances are shown for comparison to actual spectra shown in Figure 1. Fits are shown for data at 10, 20, 30, and 40 °C.

plified by reduction to sets of two-site exchanges by assuming that some of the rate constants are zero. PF4 is no exception, and we have neglected rate constants for direct monomer–tetramer exchange since it seems logical to assume that tetramers form from dimers. In effect, it has been assumed that the probability of a tetramolecular collision for direct monomer to tetramer formation is miniscule at these protein concentrations and solution conditions. This leaves two sets of exchange rate constants; one for monomer–dimer exchange and one for dimer–tetramer exchange. Moreover, of the two possible PF4 dimers which could form in solution (St. Charles et al., 1989), one of them is highly thermodynamically favored over the other (Mayo & Chen, 1989). For this reason, D in eq 1 stands for the preferred dimer only. The presence of a second "hidden" dimer population cannot be ruled out. However, a thorough analysis of PF4 aggregate equilibria under various solution conditions, i.e., pH and ionic strength, revealed no evidence for a "second" dimer population (Mayo & Chen, 1989). Therefore, we shall assume that if it does exist, its population is relatively very small and will have little, if any, effect on results discussed below.

Equilibrium Thermodynamics. Figure 1 shows representative ^1H NMR spectra of PF4 as a function of temperature from 10 to 70 °C. The approximate ^1H NMR time cutoff for slow exchange at 500 MHz is about 100 s^{-1}. Therefore, at temperatures below about 50 °C, observation of individual resonances for M, D, and T states indicates that exchange rates significantly slower than about 100 s^{-1} must exist for PF4 aggregate species. As the temperature is raised, exchange rates increase up to and then past this cutoff rate, and by 70 °C, one resonance is observed for the average of all fast-exchanging aggregate species. For thermodynamic and kinetic analyses done in this paper, the working range, therefore, is defined from these spectra as 10–40 °C.

As is evident in Figure 1, varying the sample temperature from 10 to 40 °C produces only slight differences in M–D–T populations. Qualitatively, this relates to a weak temperature dependence in aggregation equilibrium constants and, therefore, a relatively small enthalpic contribution to aggregation.

The temperature dependence of steady-state M–D–T PF4 populations was derived from Gaussian/Lorentzian fitting of relatively well-resolved Y60 3,5 ring proton resonances labeled in Figure 1. Typical fits representing the sum of three Gaussian lines, one for each M, D, and T-Y60 3,5 resonance, are shown in Figure 2 for data presented in Figure 1. Only the superposition of M, D, and T-Y60 3,5 resonance fit simulations is shown in Figure 2.

Resulting resonance area integrals from these fits gave relative M–D–T aggregate populations which were then related to steady-state concentrations from knowledge of the PF4 protein concentration per mole of Y60 in each state. These steady-state concentrations allowed dimer and tetramer association equilibrium constants, K_D and K_T, respectively, to be calculated according to eq 2. In Figure 3, the natural

$$K_D = [D]/[M]^2 \text{ and } K_T = [T]/[D]^2 \qquad (2)$$

logarithm of K_D and K_T is given versus the inverse temperature in degrees kelvin. These van't Hoff plots indicate that the slopes for dimer and tetramer association are different in sign and magnitude; therefore, enthalpic contributions to dimerization and tetramerization will be different.

Enthalpy values, $\Delta H°$, derived from these data (Figure 3) are listed in Table I along with the Gibb's free energy, $\Delta G°$,

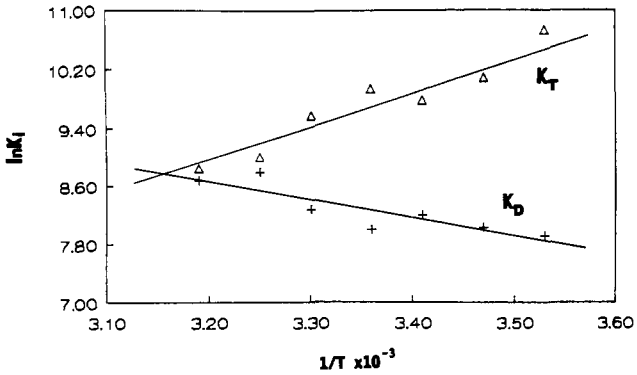

FIGURE 3: van't Hoff plots for PF4 dimer and tetramer association. The natural logarithm of K_D and K_T as defined by eq 2 and described in the text is plotted versus the inverse temperature in kelvin. The slope in these plots is proportional to the enthalpic contribution to the equilibrium free energy of association for dimerization and tetramerization.

Table I: Equilibrium Thermodynamic Parameters for PF4 Association/Dissociation

	M + M ⇌ D	D + D ⇌ T
$\Delta G°$ (kcal/mol)[a]	−5.1 ± 0.2[b]	−5.3 ● 0.4
$\Delta H°$ (kcal/mol)	+2.6 ● 1	−7.5 ± 1
$\Delta S°$ [cal/(mol·K) or eu]	+26 ± 7	−7 ± 3

[a] Value given for 30 °C. [b] Standard deviations of three or more experiments.

of association calculated from equilibrium constants, K_{eq}, according to eq 3 where R is the gas constant and T is the

$$\Delta G° = -RT \ln K_{eq} \quad (3)$$

temperature in kelvin. The entropic contribution, $\Delta S°$, to association, as given in Table I, was calculated by using

$$\Delta S° = (\Delta H° - \Delta G°)/T \quad (4)$$

Temperature Dependence of Half-Height Line Widths. Monomer and tetramer Y60 3,5 resonances can be observed in the absence (greater than 90–95%) of other aggregate species by varying the PF4 concentration (Mayo & Chen, 1989). Relative to spectra shown in Figure 1, M-Y60 and T-Y60 resonance half-height line widths, $\Delta\nu_{1/2}$, are generally smaller than when present together. This is especially obvious for the M-Y60 (3,5) resonance where $^3J_{\delta\epsilon}$ spin–spin splitting can even be observed when mostly monomer PF4 is present (Mayo & Chen, 1989). In cases of moderately slow exchange (Jardetzky & Roberts, 1981), resonance lines are broadened by an amount proportional to the rate of exchange or to the steady-state flux rate out of the state observed, i.e., inverse of the lifetime of that state. Since considerable resonance broadening is observed, exchange rates must be on the order of about 2–5 times less than the 500-MHz ^{1}H NMR exchange time cutoff of about 100 s^{-1}, i.e., slow intermediate exchange. Complete intermediate exchange would give only one broadened resonance as exchange rates move closer to the NMR exchange time cutoff given above and as shown, for example, for 60 °C in Figure 1. Real slow exchange would show only individual species with no apparent resonance broadening in aggregate species.

A mathematical expression for this is shown in eq 5 for exchange out of the monomer state into the dimer state where

$$\pi(\Delta\nu^{M'}{}_{1/2} - \Delta\nu^{M}{}_{1/2}) = (P_D/P_M)k_{DM} \quad (5)$$

$\Delta\nu^{M'}{}_{1/2}$ is the monomer half-height line width in the presence of exchange and $\Delta\nu^{M}{}_{1/2}$ is the monomer half-height line width in the absence of exchange. k_{DM} is the rate of exchange from the dimer to the monomer state, and P stands for the population in monomer, M, and dimer, D, states. These populations are readily available from resonance fit analyses for M, D, and T states as discussed above. A similar expression can be written for exchange out of the tetramer state.

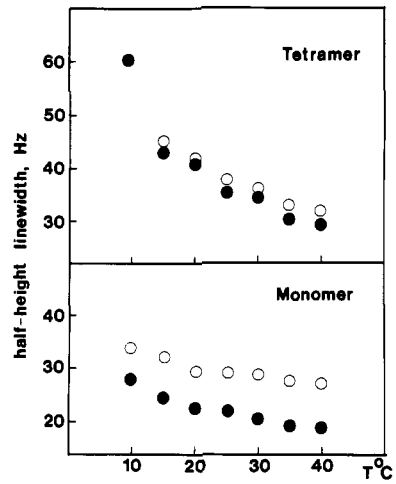

FIGURE 4: Temperature dependence of $\Delta\nu_{1/2}$ and $\Delta\nu'_{1/2}$. Line width half-heights were estimated from actual NMR spectra or from line-shape analyses as described under Materials and Methods. Line widths are shown for monomer and tetramer Y60 3,5 resonances in the presence (○) and absence (●) of exchange broadening.

Figure 4 plots the temperature dependence of apparent half-height line widths for monomer and tetramer species in the presence, $\Delta\nu'_{1/2}$, and apparent absence, $\Delta\nu_{1/2}$, of exchange. The open circles in each plot represent the apparent line width in the presence of exchange, and the closed circles represent the apparent line width in the absence of exchange. For monomer species, the difference between $\Delta\nu_{1/2}$ and $\Delta\nu'_{1/2}$ is about 5–10 Hz. Given M and D populations, this translates to exchange rate fluxes in the 10–50 s^{-1} range. Since line-width differences and M/D populations change little with temperature, this indicates a relatively small enthalpic contribution to activation energies. These data will be given and discussed later in this paper. For tetramer species, the difference between $\Delta\nu_{1/2}$ and $\Delta\nu'_{1/2}$ is considerably less, on the order of 1–2 Hz and sometimes not even measurable. Effectively, given D/T populations, this means that exchange flux rates out of the tetramer state are on the order of 1–10 s^{-1}. In this case, the derivation of the temperature dependence of tetramer exchange rates generally could not be accurately derived. Since PF4 aggregate exchange lies in the slow moderate regime on the NMR time scale, however, saturation-transfer experiments can also be performed to determine exchange rates and, in the case of tetramer PF4, apparently more accurately as discussed below.

Saturation-Transfer and Association/Dissociation "Jump-Rates". Forsén and Hoffman (1964) have given the general form of the coupled differential equations describing the time dependence of exchanging systems. For a system consisting of three magnetically nonequivalent sites, i, j, and k, with populations p_i, p_j, and p_k, the specific form of the equation is

$$dI_i/dt = -(k_{ij} + k_{ik} + \rho_i)(I_i - I_i^0) + k_{ji}(I_j - I_j^0) + k_{ki}(I_k - I_k^0) \quad (6)$$

where ρ_i is the inverse spin–lattice relaxation rate (T_1) for site i, k_{ij} is the first-order rate constant for exchange from site i to site j, I_i is the NMR intensity of site i at time t, and I_i^0 is

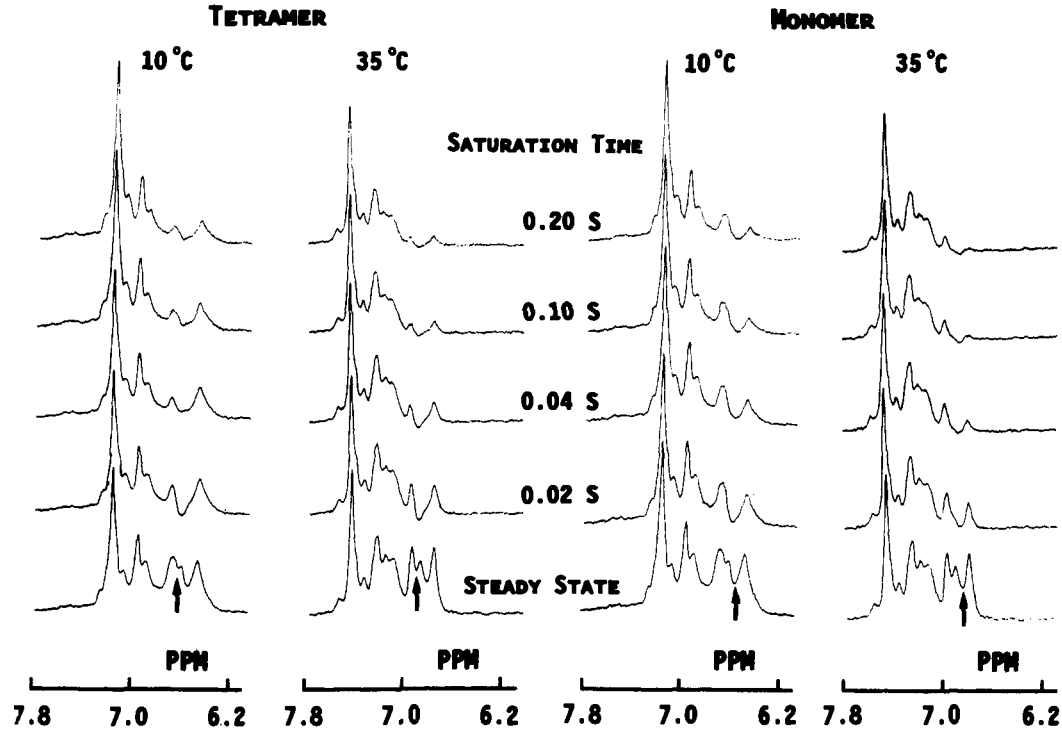

FIGURE 5: Saturation-transfer NMR spectra. ST ^{1}H NMR spectra are shown for D-Y60 3,5 resonance irradiation. The left two series are for irradiation between M- and D-Y60 3,5 resonances for use in deriving actual ST at the T-Y60 3,5 resonance (10 and 35 °C). The right two series are for irradiation between T- and D-Y60 3,5 resonances for use in deriving actual ST at the M-Y60 3,5 resonance (10 and 35 °C). Each spectrum represents 1024 time-averaged FIDs. In each case, the rf saturation time was varied for 0.02, 0.04, 0.10, and 0.20 s as indicated in the figure. The bottom spectrum in each series is a steady-state spectrum. The solution conditions are the same as discussed in the Figure 1 legend. PF4 concentration was 2.7 mg/mL.

its equilibrium intensity. Analogous equations may be written for j and k. In order to measure jump rates in this three-site system, two types of experiments must be performed: saturation transfer (ST) and spin–lattice relaxation (T_1).

In the saturation-transfer experiment where pathways to and from resonances i and k must go through resonance j, site j is saturated, and the steady-state intensities relative to off-resonance equilibrium intensities at the other sites are measured. When there is exchange, saturation of site j will decrease the intensities at the other sites, i and k, provided rates of exchange and spin–latice relaxation rates are comparable. This new equilibrium intensity, for example, for resonance i, is reached exponentially as a function of the time, t, for which resonance j is irradiated:

$$I_i(t) = I_i^0/[k_{ij}/(\rho_i + k_{ij})] \exp[-t(\rho_i + k_{ij})] + I_i^0[\rho_i/(\rho_i + k_{ij})] \quad (7)$$

At long times, t, when the new equilibrium of resonance i has been reached, eq 7 reduces to

$$I_i^\infty/I_i^0 = \rho_i/(\rho_i + k_{ij}) \quad (8)$$

For evaluation of individual PF4 exchange rate constants, only the D-Y60 3,5 proton resonance was selectively irradiated in ^{1}H ST-NMR experiments since the dimer state is intermediate in this three-site exchange case and only irradiation of the intermediary dimer state will allow measurement of single-flux rate constants. In this case, we are limited to measuring exchange flux rates into the dimer state, i.e., k_{MD} and k_{TD}. Representative ST-NMR spectra are given in Figure 5 for irradiation times of 0.02, 0.04, 0.1, and 0.2 s. Two sets of ST-NMR spectra are shown for selective irradiation at either side of the D-Y60 3,5 resonance as indicated by arrows in the figure. This was done for purposes of reducing indirect saturation at either the M- or the T-Y60 3,5 resonances as discussed below. Gaussian/Lorentzian line fittings of remaining M- and T-Y60 3,5 proton resonances in individual spectra were then done as described under Materials and Methods. ST-NMR data acquired for 10 and 35 °C are shown.

By comparison with the steady-state spectrum given at the bottom of each series in Figure 5, it is apparent that intensities at other resonances are affected by saturation of the D-Y60 3,5 resonance. These intensity changes are due to three effects: (1) actual saturation transfer between exchanging resonance populations; (2) indirect saturation of resonances proximal in chemical shift to the saturated resonance; and (3) nuclear Overhauser effects at Y60 2,6 ring proton resonances. Since we are only interested in actual ST at M- and T-Y60 3,5 resonances, only the unwanted effect of indirect saturation concerns us. Indirect saturation arises when, for example, the dimer resonance is saturated by rf whose power spectrum has a finite width which overlaps with other closely positioned resonances. In this case, Y60 3,5 M and D, and D and T resonances are only separated by about 0.11 ppm, and one can expect indirect saturation to occur.

To minimize effects from indirect saturation, the irradiating frequency was stepped through the D-Y60 3,5 resonance. In this way, the effective irradiating frequency was at some point furthest away from a neighboring M- or T-Y60 3,5 resonance while still saturating the D-Y60 3,5 resonance. For example, if we are interested in observing less indirect saturation at the M-Y60 3,5 resonance, then placing the irradiating rf between the D-Y60 and T-Y60 3,5 resonances gives less indirect saturation at the M-Y60 3,5 resonance. ST-NMR data shown in Figure 5 have been generated in this way.

Stepping through the D-Y60 3,5 resonance does not, however, eliminate indirect saturation. Correction for indirect

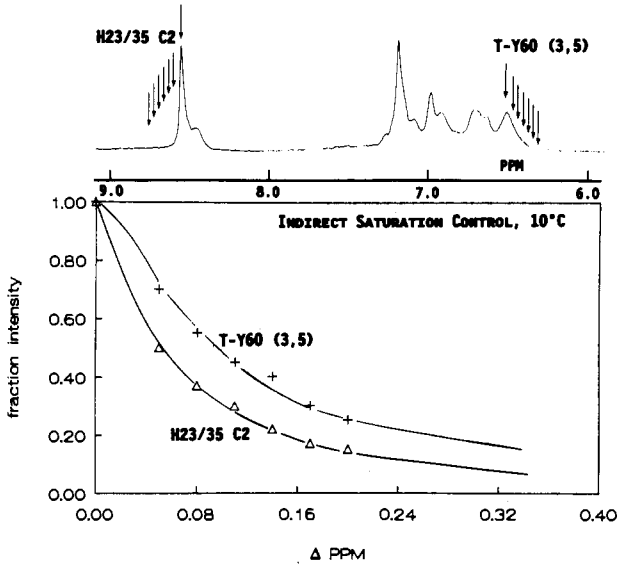

FIGURE 6: ST-NMR control for indirect saturation. The fractional resonance intensity changes for indirect saturation control T-Y60 3,5 and H23/35 C2 resonances are plotted versus the frequency difference from the respective resonance saturated. At the top of the figure is shown a normal NMR spectrum where arrows indicate rf irradiations as plotted in the figure. These control values are for 10 °C and an irradiation time of 0.2 s for the maximum values of indirect saturation. Solid lines through data points are drawn only as visual aids.

saturation was accomplished by placing the irradiating rf at varying frequencies at the upfield side of the T-Y60 3,5 resonance and then at the downfield side of the H23/35 C2 resonance in order to generate a plot of fractional resonance intensity change versus the frequency difference from the control resonance. This allows sampling of the irradiating field width at control resonance positions where line widths are significantly different from each other. In these cases, one would expect the narrower control resonance, i.e., H23/35 C2, to show consistently less indirect saturation; this has been observed. These control data are exemplified in Figure 6. A frequency difference of zero, and therefore a fractional intensity change of 1, means that the irradiating rf was placed directly, for example, on the T-Y60 3,5 resonance which was subsequently nulled. As the frequency difference between the T-Y60 3,5 resonance and the irradiating rf was increased, i.e., moved further upfield from the T-Y60 3,5 resonance (indicated by arrows in the 1D spectral trace at the top of the figure), the fractional intensity change decreased, and therefore more of the original T-Y60 3,5 resonance intensity remained after rf irradiation. At these control conditions, 40% of the T-Y60 3,5 resonance was nulled at a frequency difference of 0.11 ppm, the same frequency difference as that found between D and T resonances. In this way, indirect saturation of the T-Y60 3,5 resonance by D-Y60 3,5 resonance irradiation and actual ST from the T-Y60 3,5 resonance could be estimated. This type of control was done for each set of conditions and with each set of ST-NMR experiments. Even varying the length of irradiation time gave different indirect saturation control results. Since the M-Y60 3,5 resonance was generally narrower than the T-Y60 3,5 resonance, the narrower H23/35 C2 control resonance was used for correction of indirect saturation at the M-Y60 3,5 resonance. Sometimes an approximate correction for the M-Y60 3,5 resonance was used when its apparent line width fell between that of either control resonance. Depending on temperature, i.e., resonance line width, and length of resonance saturation time, indirect effects accounted for about 20–60% of intensity changes on irradiation of the D-Y60 3,5 resonance. Data were also collected at various PF4 concentrations where MDT resonance intensities could be varied in order to better gauge the effectiveness of this approach.

Figure 7 gives some ST-NMR-derived plots of M-Y60 and T-Y60 fractional intensity changes due to D-Y60 3,5 resonance saturation as a function of the irradiation time (crosses). In the same plot is shown the fraction of indirect saturation estimated from control data (triangles) discussed above (Figure

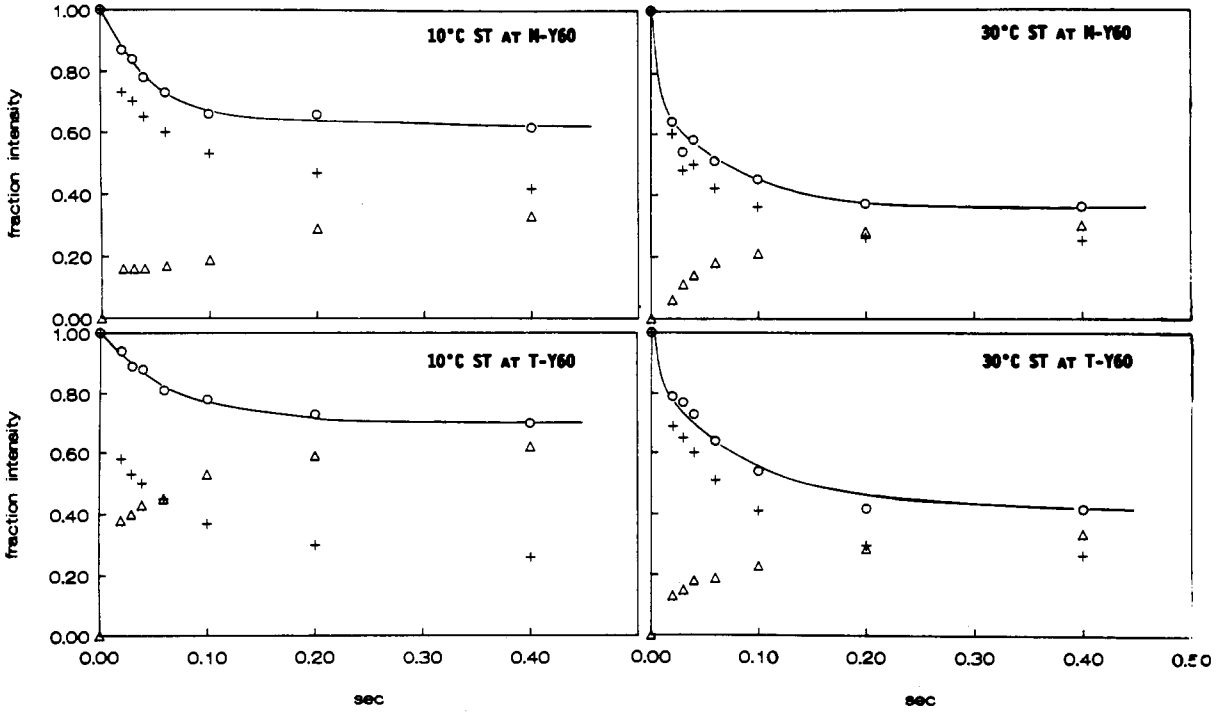

FIGURE 7: Time development curves for saturation transfer. Sample data for the time development of saturation transfer at M-Y60 and T-Y60 3,5 resonances are shown. The fractional intensity change of M-Y60 3,5 and T-Y60 3,5 resonances is shown versus the time of irradiation (data indicated by "+" symbols). The values of indirect saturation used for correction of these fractional intensity changes are also shown ("Δ" symbols) as discussed in the text. The actual ST values corrected according to eq 9 are also plotted ("O" symbols).

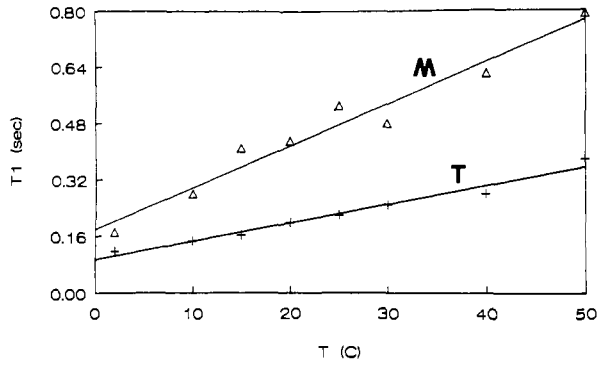

FIGURE 8: Temperature dependence of T_1 for M- and T-Y60 3,5 resonances. T_1 values for M- and T-Y60 3,5 resonances were experimentally derived as explained under Materials and Methods. Here, these values are plotted versus the temperature in degrees Celsius. The data points have been least-squares-fitted as shown in the figure.

6) at the respective resonance and the actual ST (corrected) (circles). The actual ST was calculated by using eq 9 where

$$I(t)/[I_0(1-f)] \quad (9)$$

$I(t)$ is the area of the M-Y60 or T-Y60 3,5 resonance on saturation of the D-Y60 3,5 resonance for a length of time t, I_0 is the steady-state area of the M-Y60 or T-Y60 3,5 resonance, respectively, and f is the fractional area change of the M-Y60 or T-Y60 3,5 resonance due to indirect saturation. These actual ST values correspond to I_i in eq 6–8.

The second parameter necessary to derive individual jump rates is the spin–lattice relaxtion time, T_1, i.e., the inverse of ρ_i in eq 6–8. Derivation of T_1 values at pH 4, where all states are simultaneously present, yielded T_1 values that were nearly all the same due to the exchange process. For this reason, T_1 values were derived from NMR data taken at a slightly lower pH value of 3.5 where M and T states could be observed in the absence (greater than 90–95%) of the other by varying the PF4 concentration (Mayo & Chen, 1989). The T_1 temperature dependence for M-Y60 and T-Y60 3,5 resonances is shown in Figure 8. T_1 for the M-Y60 3,5 resonance ranges from 0.17 s at 2 °C to 0.8 s at 50 °C. T_1 for the T-Y60 3,5 resonance is 0.12 s at 2 °C and increases less sharply to 0.36 s at 50 °C. We have assumed that the temperature dependence of T_1 data in this range is linear; therefore, data have been least-squares-fitted as shown by the linear curve in the figure. While it is difficult to fully assess why M-Y60 and T-Y60 3,5 resonances show a significantly different T_1 temperature slope, it is normal to observe relatively longer T_1 values for lower molecular weight species. Moreover, it is known that Y60 is more solvent-exposed, and therefore presumably more mobile in monomer PF4 (Mayo & Chen, 1989). This might as well account for part of the difference in T_1 values.

By use of these T_1 data, eq 7 was least-squares-fitted to actual ST data as shown in Figure 7 by the solid curve, and jump rates for M to D association, k_{MD}, and T to D dissociation, k_{TD}, were thereby derived. By knowing these two jump rates, the remaining two jump rates, k_{DM} and k_{DT}, were calculated from steady-state populations according to eq 10

$$A_D/A_M = k_{MD}/k_{DM} \text{ and } A_T/A_D = k_{DT}/k_{TD} \quad (10)$$

where A stands for the steady-state resonance area of an aggregate species (corrected for the number of Y60 residues per aggregate species) according to respective subscripts, and k stands for the jump rate as defined in eq 1.

The temperature dependencies of all four jump rates are given in Figure 9A. Individual jump rates generally increase weakly with increasing temperature. Bar lines with some of the data points indicate the standard deviation from the average of at least three data sets (derived from both ST-NMR and line-broadening data) collected at various PF4 concentrations. Dimer–tetramer jump rates estimated from exchange-induced line broadening were about the same as those derived from ST-NMR experiments, while exchange-induced line broadening generally placed monomer–dimer jump rates in the upper range, i.e., normally larger than those derived from ST-NMR measurements. All values have been averaged together since they were, in any event, in a similar range showing similar trends. This, in effect, accounts for the larger standard deviation in overall monomer–dimer jump rates.

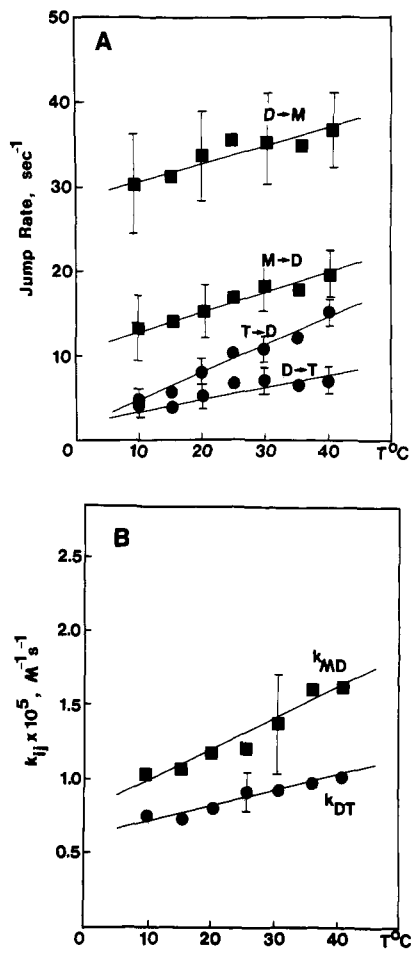

FIGURE 9: Temperature dependencies of jump rates and rate constants. The temperature dependence of jump rates k_{TD} and k_{MD} which were experimentally derived by ST ^{1}H NMR and exchange broadening is indicated in panel A. The temperature dependence of jump rates k_{DM} and k_{DT} is also plotted; these have been estimated according to eq 10 from M–D–T Y60 3,5 resonance population ratios and experimental values of k_{TD} and k_{MD} and as discussed in the text. Association rate constants in M^{-1} s^{-1} units (panel B) were derived from respective jump rates and equilibrium population concentrations as discussed in the text. Vertical lines drawn through some of the data indicate typical standard deviations from the average of at least three different experiments.

Steady-state rate constants for unimolecular dissociation of dimers and tetramers are given by their respective jump rates. The association rate constants for dimer and tetramer formation were calculated from equilibrium constants. These values were essentially the same as dividing association jump rates by the respective M or D steady-state concentration. The temperature dependencies of these values are plotted in Figure 9B. Standard deviations from the average of these data are in the 20–30% range as exemplified by line bars for values at 25 and 30 °C.

Table II: Activation Thermodynamic Parameters for PF4 M–D–T States

	M → D	D → M	D → T	T → D
ΔG^* (kcal/mol)	+10.5 ± 0.6[b]	+15.6 ± 0.4	+11.1 ± 0.3	+16.3 ± 0.5
ΔH^* (kcal/mol)	+2.9 ± 1	+0.6 ± 0.4	+0.9 ± 0.6	+5.9 ± 1.2
ΔS^* [cal/(mol·K) or eu]	−25 ± 7	−50 ± 8	−35 ± 5	−33 ± 8

[a] Values given for 30 °C. [b] Standard deviations of three or more experiments.

Table III: Expected Signs of Contributions to $\Delta H°$ and $\Delta S°$ [a]

process	$\Delta H°$	$\Delta S°$
hydrophobic association[b]	pos	pos
ionic (charge neutralization)	slight pos or neg	pos
van der Waals	neg	neg
H-bond formation in low dielectric medium	neg	neg
protonation	neg	neg

[a] Data taken from Klotz (1973) and from Ross and Subramanian (1981). [b] By hydrophobic association, only reference to the partial withdrawal of a nonpolar group from water is made and not to any further interaction between nonpolar groups themselves.

From these kinetic data, transition free energy, i.e., ΔG^*, values were calculated by using eq 11 given by Laidler (1979)

$$\Delta G^*_{ij} = -RT \ln (k_{ij}h/k_BT) \quad (11)$$

where ΔG^*_{ij} is the activation (transition) free energy from state i to state j, R is the universal gas constant, T is the temperature in kelvin, k_{ij} is the associated jump rate, h is Planck's constant, and k_B is the Boltzmann constant. From eq 4, it is apparent that $\Delta G^*/T = \Delta H^*/T - \Delta S^*$. Therefore, Arrhenius plots of $\Delta G^*/T$ versus $1/T$ were made (linear plots not shown) in order to estimate activation enthalpies and entropies. These activation thermodynamic parameters are listed in Table II for data (±SD) at 30 °C. It should be noted that a 50% deviation in k corresponds to less than a 0.5 kcal/mol variance in activation free energy values. Our standard deviations generally ran about half that value, i.e., 20–30%.

Discussion

Thermodynamic parameters derived for PF4 association/dissociation in this paper represent sum totals of the various contributions to enthalpy and entropy terms. A general summary of the signs for thermodynamic parameters and their accepted interpretations (Klotz, 1973; Ross & Subramanian, 1981) is given in Table III.

The equilibrium thermodynamics of PF4 indicate that favorable association of dimers and tetramers, i.e., a negative free energy term, is the result of different forces in each association step. Dimer association is entropy-driven since the enthalpy contribution is a small positive number, and the entropy contribution is +26 eu. Positive entropy and enthalpy values generally indicate hydrophobic interactions or electrostatic interactions in a medium of low dielectric constant, i.e., association of charged groups (salt-bridge formation) excluded from the polar solvent or environment as in the interior of a protein. In PF4 dimers of the AC type, both hydrophobic contacts and solvent-excluded salt bridges form the basis for monomer–monomer interactions (St. Charles et al., 1989; Mayo & Chen, 1989). These thermodynamic values, therefore, are consistent with known structural data for PF4.

Although formation of two salt bridges in monomer–monomer association contributes about −10 kcal/mol to the enthalpy of association (Ghelis & Yon, 1982), an apparent enthalpy change of +2.5 kcal/mol is observed. In this case, the breaking of protein–water molecule H bonds at the monomer surface binding site during dimerization could give rise to an enthalpy value of about +12.5 kcal/mol (dimer) that would offset the expected negative value from salt-bridge formation. A similar interpretation was made for α-chymotrypsin dimerization (Kitano et al., 1989). This could account for displacement of about four water molecules from the dimer intersubunit interface. This number is in the range found for crystal water bound to proteins from X-ray data analysis (Blevins & Tulinsky, 1985). In the case of α-chymotrypsin, 40–70 water molecules have been reported to be bound at the surface (Birktoff & Blow, 1972). This number, however, is for the total surface of α-chymotrypsin; in the case of PF4 dimers, we are only dealing with a fraction of the monomer surface. Moreover, the positive entropy value also suggests that water molecules are released during dimerization. In support of this, Thompson and Lakowicz (1984) reported that the self-association of melittin is driven by intersubunit hydrophobic interactions and the release of water molecules at the time of association.

Negative enthalpy and entropy values as observed here for dimer–dimer (tetramer) association generally indicate hydrogen-bonding interactions (see Table III). Structurally, this is known to be the case with AC-type dimer–dimer associations, i.e., AB subunit interactions (St. Charles et al., 1989; Mayo & Chen, 1989). Once again, these thermodynamic values are consistent with the structural picture of PF4. A total of 12 intersubunit, antiparallel β-sheet hydrogen bonds (H bonds) are formed on dimer–dimer association (St. Charles et al., 1989). Each H bond formed in an environment of low dielectric constant is an important source of negative contribution to ΔH^0 and ΔS^0 (Pimentel & McClellan, 1971). Typical values for such processes are −5 kcal/mol for ΔH^0 and −10 to −20 eu for ΔS^0 (Pimentel & McClellan, 1971). The 12 H bonds known to form at the dimer–dimer interface should therefore produce about −60 kcal/mol in ΔH^0 and about −120 to −240 eu in ΔS^0. Apparent ΔH^0 and ΔS^0 values of −7.5 kcal/mol and −7 eu, respectively, as observed here suggest that another (other) process(es) is (are) also occurring. To account for this difference, positive contributions to apparent ΔH^0 and ΔS^0 values must also be present. Only two types of interactions are known to produce positive enthalpy and entropy contributions: hydrophobic and electrostatic/ionic (Table III). Specific electrostatic/ionic interactions are apparently absent from dimer–dimer interactions; however, hydrophobic residue interactions are known to be present at the dimer–dimer interface (St. Charles et al., 1989). Therefore, part of the ΔH^0 value must be due to hydrophobic interactions. Assuming that the hydrophobic effect is the only contribution, it must contribute about +52 kcal/mol and +112 to +232 eu to ΔH^0 and ΔS^0, respectively. These enthalpy and entropy values are surprisingly large. In any event, the major driving force in dimer–dimer association is H-bond formation, but not by much.

At 30 °C, rate constants for PF4 monomer–monomer (k_{MD}) and dimer–dimer (k_{DT}) associations are $(13 \pm 4) \times 10^4$ and $(8 \pm 2) \times 10^4$ M^{-1} s^{-1}, respectively. Dimer (k_{DM}) and tetramer (k_{TD}) dissociation rate constants are 35 ± 10 and 6 ± 2 s^{-1}, respectively. The equilibrium association constant for tetramer formation (K_T) is, therefore, about 5 times larger than that for dimer formation (K_D). The primary reason for this difference is now known to be the result of slower tetramer dissociation or, in other words, a longer lived tetramer state.

The association/dissociation kinetics for α-chymotrypsin dimerization have been studied by stopped-flow spectropho-

tometry (Kitano et al., 1989). For this two-state exchange process at pH 4.3 and 25 °C, association and dissociation rate constants are 1.3×10^3 M^{-1} s^{-1} and 0.7 s^{-1}, respectively, yielding an association equilibrium constant of 1.9×10^3 M^{-1}. As measured by Koren and Hammes (1975), these parameters for α-chymotrypsin are in the same range, i.e., 3.7×10^3 M^{-1} s^{-1}, 0.7 s^{-1}, and 5.5×10^3 M^{-1}, respectively. The enthalpy and entropy contributions to the equilibrium free energy of association in α-chymotrypsin [−4.4 kcal/mol (25 °C)] are both positive, i.e., +4.6 kcal/mol and +30 eu, respectively (Kitano et al., 1989), as they are for PF4 dimerization. While the PF4 equilibrium K_D value is similar, the association rate constant, k_{MD}, is about 10–15 times larger for PF4. The PF4 dimer dissociation rate constant, k_{DM}, also being larger, compensates in terms of yielding similar equilibrium association constants. Comparatively, these differences in protein–protein exchange kinetics are surprising since monomer–monomer interactions for PF4 and α-chymotrypsin involve the formation of two, low dielectric medium, intersubunit salt bridges and hydrophobic interactions. Interestingly, while activation free energies are also comparable, i.e., $\Delta G^*_{forward} = +13.3$ kcal/mol and $\Delta G^*_{reverse} = +17.7$ kcal/mol for α-chymotrypsin, activation association entropies are positive for α-chymotrypsin while they are negative for PF4 dimerization (see Table II). This entropy difference originates from use of the Arrhenius reaction rate theory and is, therefore, consistent with faster kinetics for PF4 association/dissociation. The main difference in these parameters seems to lie in the activation subunit association entropy term. Such comparisons, however, are difficult to make on an absolute scale, since solution conditions are somewhat different, i.e., temperature, pH, ionic strength. For example, a 5 °C change in temperature would produce somewhat faster association/dissociation rates in PF4 dimerization, although clearly not by a factor of 10–15. Furthermore, 10 mM KCl (among other reagents) is present in the α-chymotrypsin sample; if this were added to the PF4 sample, flux rates into or out of the dimer/tetramer state would be considerably different from those measured in this paper (Mayo & Chen, 1989). The net effect of increased ionic strength on the PF4 aggregation process would be to increase tetramer populations. In any event, this too does not fully explain association/dissociation kinetic differences between PF4 and α-chymotrypsin.

As is the case here with PF4 and α-chymotrypsin, it is interesting to note that ligand association/dissociation kinetics vary considerably even among proteins of similar molecular weight. For example, melittin dimer and tetramer association/dissociation rate constants (salt dependent) are $(1–3.8) \times 10^{-5}$ M^{-1} s^{-1} and $(30–4) \times 10^{-3}$ s^{-1}, respectively (Schwarz & Beschiaschvili, 1988). The insulin receptor system yields initial association and dissociation rate constants of from 1.6×10^5 M^{-1} s^{-1} (Lipkin et al., 1986) to 2×10^6 M^{-1} s^{-1} (Corin & Donner, 1982) and $(2–4) \times 10^{-3}$ s^{-1} (Lipkin et al., 1986; Corin & Donner, 1982), respectively, while for the epidermal growth factor receptor system, values of 1.2×10^6 M^{-1} s^{-1} and 2×10^{-2} s^{-1}, respectively, are found (Mayo et al., 1989). Some recent examples of small molecule–protein interactions give association/dissociation rate constants of 3.3×10^5 M^{-1} s^{-1} and 1×10^{-4} s^{-1}, respectivley, from the Tet-repressor–tetracycline complex (Takahashi et al., 1986) and 1.3×10^4 M^{-1} s^{-1} and 3.2×10^{-2} s^{-1}, respectively, for carbohydrate binding to basic lectin (Khan et al., 1986). The association rate constant for the interaction of relatively low molecular weight *N*-(phosphonacetyl)aspartate with the catalytic subunit of aspartate transcarbamoylase (Cohen & Schachman, 1986), at the low molecular weight extreme, is 9×10^7 M^{-1} s^{-1}. Usually, a typical range for protein–ligand (low molecular weight) association rate constants is $10^6–10^8$ M^{-1} s^{-1} (Fersht, 1977).

Association rate constants, at least in their overall trend, tend to more or less comply with diffusion-limited rate theory (De Lisi & Weigel, 1981). The actual magnitude of association rate constants, however, is normally lower than diffusion-limited rate theory would predict. This indicates that simple molecular diffusion is not the only factor controlling association reactions. This is not too surprising since the De Lisi and Weigel estimate is based on the Stokes–Einstein model which assumes diffusion of hard spherical molecules in the absence of solvent effects like hydrogen bonding and electrostatic interactions with the solvent or between protein molecules. Generally, for systems discussed above, there is little or no correlation between molecular weight and dissociation rates. Dissociation is controlled by the relative strength of the paired ligand–receptor interaction and by the sum of forces (collisions) necessary to provide the energy to separate them. PF4 dissociation, therefore, is relatively easy to induce at pH 4. At pH 7 in the presence of 0.2 M NaCl, the equilibrium constant for PF4 tetramer formation is about 100 times larger than that at pH 4 in the absence of added NaCl. If we assume that the association rate constant of 1×10^5 M^{-1} s^{-1} is about the same under these more physiologic conditions, then the tetramer dissociation rate constant of 7 s^{-1} at pH 4 will be reduced to about 7×10^{-2} s^{-1} by pH 7, 0.2 M NaCl. This value is now more in the range of dissociation rate constants observed for ligand–receptor binding in systems studied at pH 7 and mentioned above.

By itself, the release of water molecules driving the PF4 association process is inconsistent with the negative activation entropy derived for PF4 dimerization. Dimer dissociation activation entropy compensates for this in overall thermodynamic terms by being more negative. Moreover, since we are dealing with the sum of thermodynamic terms, the net negative activation entropy term probably indicates a contribution from another (other) source(s). Part of the negative activation entropy comes from general ordering of monomer subunits. Other normally invoked processes which could account for this are not readily apparent. Protein flexibility/dynamics/folding may provide at least part of the answer. Configurational entropy (de Gennes, 1979), which has been known for some time to be a contributor to protein folding destabilization, could contribute to relatively fast dissociation kinetics and a negative association activation entropy term. Basically, this term arises from the fact that a peptide chain can occupy a large volume of space in any of a large number of different configurations. Because the folding of a protein involves collapse of the chain from a large volume (denatured state) to a small volume (native state), the protein must lose a considerable amount of entropy in the process. In some ways, the possible contribution of configurational entropy or the like to these processes is consistent with what we know so far about PF4 structure/dynamics. Several observations suggest that PF4 has a rather "loose" structure in the sense of large-amplitude, backbone fluctuations. Photo-CIDNP ^1H NMR results indicate that the C-terminal α-helix domain Y60 residue in monomer PF4 is considerably more solvent-accessible than Y60 in tetramer PF4 (Mayo & Chen, 1989). Since the C-terminal segment in PF4 has a high potential for α-helix formation and this structure is found to exist at least in tetramer bovine PF4 (St. Charles et al., 1989), it is presummably maintained in monomer PF4. The greater solvent exposure

of Y60 in monomer PF4, therefore, may indicate a more open, perhaps more flexible, C-terminal domain structure, although this is still unclear. Additionally, amide proton/deuteron exchange kinetics are faster by several orders of magnitude for backbone NH protons in monomer PF4 relative to tetramer PF4 (Chen and Mayo, unpublished results). While some amide protons may be longer lived due to inclusion within the tetramer protein matrix, at least several of them are at the outside surface of the tetramer where only decreased protein backbone flexibility can explain decreased exchange rates. Moreover, analysis of X-ray diffraction data for tetramer bovine PF4 (St. Charles et al., 1989) indicates significant lattice disorder over the first 24 or so N-terminal residues, suggesting that, even in the presummably less internally mobile tetramer PF4, considerable flexibility is apparent. Since it is clear that additional terms need to be considered in a model for protein–protein association/dissociation, these terms should probably include some aspects of conformational flexibility, which in the case of PF4 may help to account for observed exchange kinetic parameters.

Registry No. PF4, 37270-94-3.

References

Aune, K. C., & Timasheff, S. N. (1971) *Biochemistry 10*, 1609–1617.

Aune, K. C., Goldsmith, L. C., & Timasheff, S. N. (1971) *Biochemistry 10*, 1617–1625.

Barber, A. J., Kaser-Glanzmann, R., Jakabova, M., & Luscher, E. F. (1972) *Biochim. Biophys. Acta 286*, 312–329.

Birktoff, J., & Blow, D. W. (1972) *J. Mol. Biol. 68*, 187–205.

Blevins, R. A., & Tulinsky, A. (1985) *J. Biol. Chem. 260*, 4264–4270.

Brindle, K. M., Porteous, R., & Radda, G. K. (1984) *Biochim. Biophys. Acta 786*, 18–24.

Brown, T. R., & Ogawa, S. (1977) *Proc. Natl. Acad. Sci. U.S.A. 74*, 3627–3632.

Cayley, P. J., Albrand, J. P., Feeney, J., Roberts, G. C. K., Piper, E. A., & Burgen, A. S. V. (1979) *Biochemistry 18*, 3886–3895.

Cohen, R. E., & Schachman, H. K. (1986) *J. Biol. Chem. 261*, 2623–2631.

Corin, R. E., & Donner, D. B. (1982) *J. Biol. Chem. 257*, 104–110.

De Gennes, P. G. (1979) in *Scaling Concepts in Polymers Physics*, Cornell University Press, Ithaca, New York.

De Lisi, C., & Wiegel, F. W. (1981) *Proc. Natl. Acad. Sci. U.S.A. 78*, 5569–5572.

Deuel, T. F., Kein, P. S., Farmer, M., & Heinrikson, R. L. (1977) *Proc. Natl. Acad. Sci. U.S.A. 74*, 2256–2258.

Deuel, T. F., Senior, R. M., Chuang, D., Griffin, G. L., & Heinrikson, R. L. (1981) *Proc. Natl. Acad. Sci. U.S.A. 78*, 4584–4587.

Faller, J. W. (1973) in *Determination of Organic Structures by Physical Methods* (Nachod, F. C., & Zuckerman, J. J., Eds.) Vol. 5, Chapter 2, Academic Press, New York.

Fersht, A. (1977) in *Enzyme Structure and Mechanism*, pp 130–131, W. H. Freeman and Co., San Francisco.

Forsén, S., & Hoffman, R. A. (1964) *J. Chem. Phys. 40*, 1189–1195.

Ghelis, C., & Yon, J. (1982) in *Protein Folding*, pp 136–176, Academic Press, New York.

Hermodson, M., Schmer, G., & Kurachi, K. (1977) *J. Biol. Chem. 252*, 6276–6279.

Jardetzky, O., & Roberts, G. C. K. (1981) *NMR in Molecular Biology*, Academic Press, New York.

Khan, M. I., Sastry, M. V. K., & Surolia, A. (1986) *J. Biol. Chem. 261*, 3013–3019.

Kitano, H., Maeda, Y., & Okubo, T. (1989) *Biophys. Chem. 33*, 47–54.

Klotz, I. M. (1973) *Ann. N.Y. Acad. Sci. 226*, 18–24.

Koren, R., & Hammes, G. G. (1975) *Biochemistry 15*, 1165–1173.

Laidler, K. J. (1979) in *Theories of Chemical Reaction Rates*, pp 41–55, R. E. Krieger Publishing Co. Inc., Huntington, NY.

Lipkin, E. W., Teller, D. C., & de Haëns, C. (1986) *J. Biol. Chem. 261*, 1702–1711.

Lowry, O. H., Rosbough, N. J., Fan, A. L., & Randall, R. J. (1951) *J. Biol. Chem. 193*, 265–270.

Malloy, C. R., Sherry, A. D., & Nunnally, R. L. (1985) *J. Magn. Reson. 64*, 243–254.

Mamatyuk, V. I., Derendyaev, B. G., Detsina, A. N., & Koptyug, V. A. (1974) *Russ. J. Org. Chem. 10*, 2487–2496.

Mann, B. E. (1977) *Chem. Commun.*, 626–628.

Mayo, K. H., & Chen, M. J. (1989) *Biochemistry 28*, 9469–9478.

Mayo, K. H., Nunez, M., Burke, C., Starbuck, C., Lauffenburger, D., & Savage, C. R., Jr. (1989) *J. Biol. Chem. 264*, 17838–17844.

Moore, S., Pepper, D. S., & Cash, J. D. (1975) *Biochim. Biophys. Acta 379*, 379–384.

Pimentel, G. C., & McClellan, A. L. (1971) *Annu. Rev. Phys. Chem. 22*, 347–385.

Post, C. B., Ray, W. J., Jr., & Gorenstein, D. G. (1989) *Biochemistry 28*, 548–558.

Ross, P. D., & Subramanian, S. (1981) *Biochemistry 20*, 3096–3102.

Rucinski, B. S., Niewiarowski, S., James, P., Walz, D. A., & Budzynski, A. Z. (1979) *Blood 53*, 47–62.

Schwarz, G., & Beschiaschvili, G. (1988) *Biochemistry 27*, 7826–7831.

St. Charles, R., Walz, D. A., & Edwards, B. F. P. (1989) *J. Biol. Chem. 264*, 2092–2099.

Strehlow, H., & Knoche, W. (1969) *Ber. Bunsen-Ges. Phys. Chem. 73*, 427–436.

Takahashi, M., Altschmied, L., & Hillen, W. (1986) *J. Mol. Biol. 187*, 341–348.

Thompson, R. B., & Lakowicz, J. R. (1984) *Biochemistry 23*, 3411–3418.

Ugurbil, K., Petein, M., Maidan, R., Michurski, S., & From, A. H. L. (1986) *Biochemistry 25*, 100–107.

Waddell, W. J. (1956) *J. Lab. Clin. Med. 48*, 311–314.

Walz, D. A., Wu, V. Y., de Lamo, R., Dene, H., & McCoy, L. E. (1977) *Thromb. Res. 11*, 893–898.

Wüthrich, K. (1986) *NMR of Proteins and Nucleic Acids*, Wiley Inc., New York.